NiO and CrO_x interaction promoting in situ generation of the coordinatively unsaturated Cr-O acid-base for oxygen-lean propane dehydrogenation

Yu Ren[a,b]†, Xiao Chu[a]†, Qi Cao[a], Zean Xie[a]*, Lian Kong[a], Xiaoqiang Fan[a], Xia Xiao[a] , Zhen Zhao[a,b]*

[a]Institute of Catalysis for Energy and Environment, Shenyang Normal University, Shenyang 110034, China

[b]State Key Laboratory of Heavy Oil Processing, China University of Petroleum, Chang Ping, Beijing 102249, China

†These authors contributed equally.

*Corresponding Author.

*E-mail: zhenzhao@cup.edu.cn (Z. Zhao); xiezean@126.com (Z. Xie)

Calculation method

1. To determine the space time yield of propene formation STY(C_3H_6) under an industrially relevant feed with 40 vol % propane, the tests were performed at a degree of propane conversion below 15%.

$$\text{STY}(C_3H_6) = \frac{Y_{C_3H_6} \times F_{C_3H_8} \times 42.08}{1000 \times 22.4 \times m_{cat}} \times 60$$

Here, STY(C_3H_6) is space time yield of C_3H_6 ($kg(C_3H_6)\cdot h^{-1}\cdot kg(cat)^{-1}$), m_{cat} is catalyst amount (g). $F_{C_3H_8}$ ($ml\cdot min^{-1}$) is the C_3H_8 flow rate.

2. A first-order deactivation model was used to evaluate the catalyst stability:

$$k_d = (\ln [(1-X_{final})/X_{final}] - \ln [(1 - X_{initial})/X_{intial}])/t$$

where X_{intial} and X_{fianal}, respectively, represent the conversion measured at the initial and final period of an experiment, and t represents the reaction time (h), k_d is the deactivation rate constant (h^{-1}). High k_d value means rapid deactivation, that is, low stability.

3. Our calculated lattice constant of $MgAl_2O_4$ is 8.10 Å, which is consistent with the experimental results 8.08 Å. (Materials Letters, 2004, 58(10): 1625-1628.) The conjugate gradient algorithm was used in ionic optimization and the convergence threshold was set to 10^{-6} eV in electronic relaxation and 0.01 eV/Å in Hellmann-Feynman force on each

atom. A Monkhorst-pack 9× 9× 9 k-point mesh was used for the Brillouin zone integration.

Xu et.al found that surface energies of $MgAl_2O_4$(100) are lower than $MgAl_2O_4$(110) and $MgAl_2O_4$(111) through DFT calculations, it indicates that the low-index (100) surface is the most stable and dominant. (Applied Surface Science, 2016, 376: 97-104.) Moreover, $MgAl_2O_4$(100) surface contains rich metal sites, which is suitable for studying the mechanism of catalytic reaction, therefore, we selected $MgAl_2O_4$(100) facet.

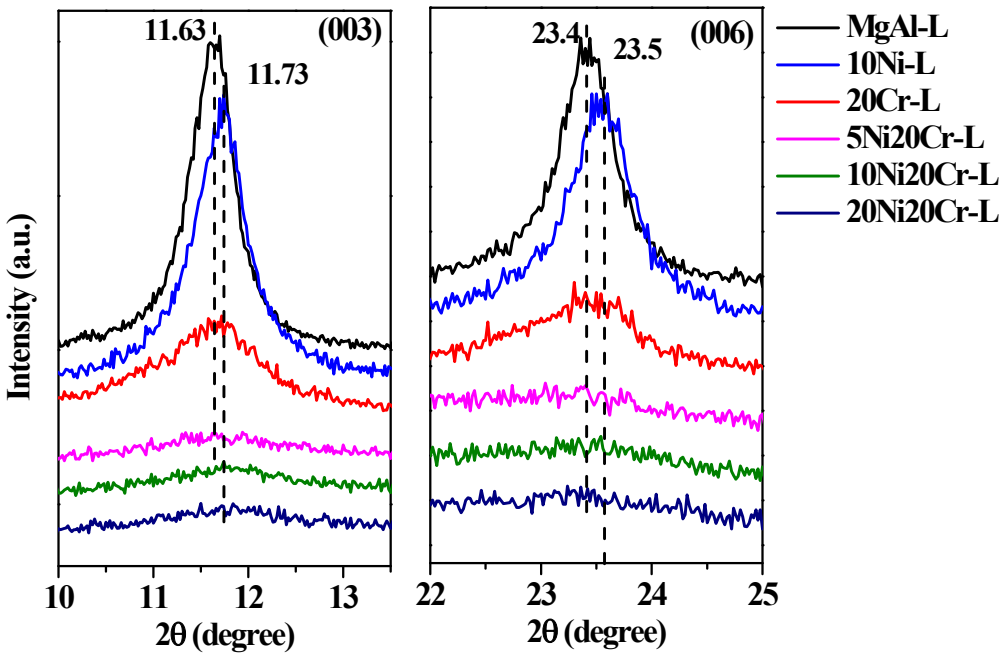

Fig. S1 XRD patterns of the MgAl-L, 10Ni-L, 20Cr-L and xNi20Cr-L catalysts with different Ni content.

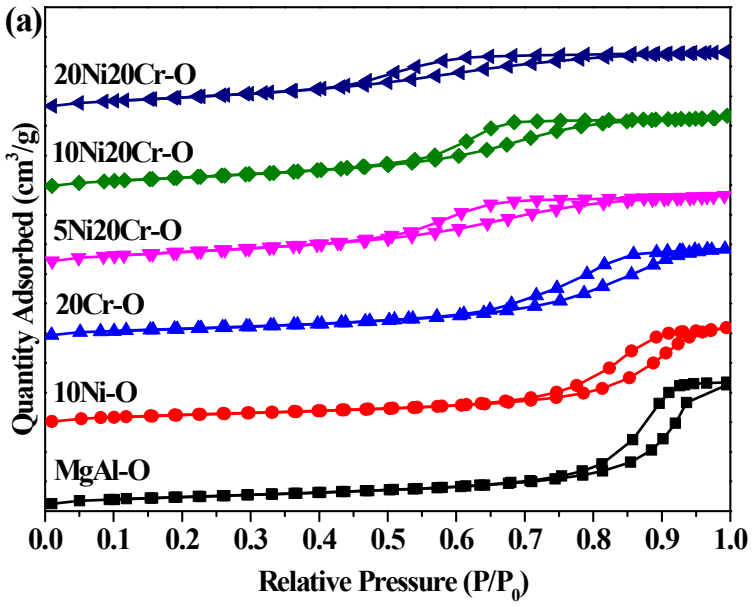

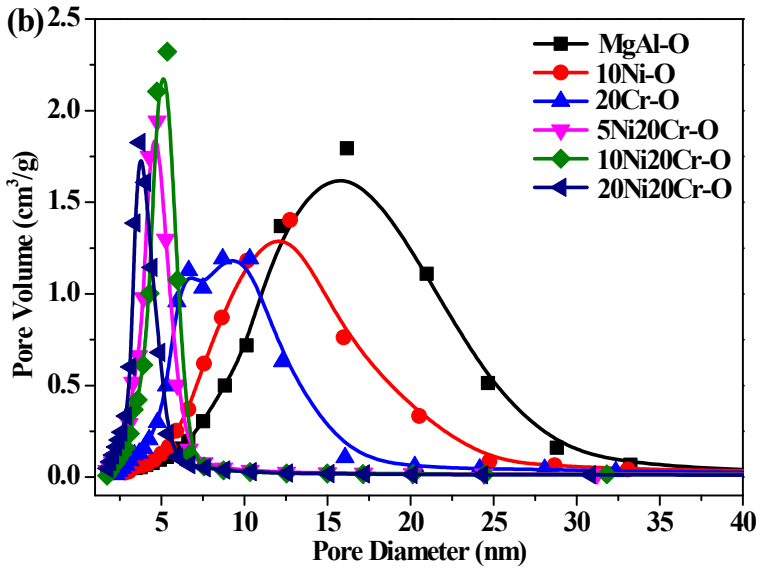

Fig. S2. (a) N_2 adsorption-desorption isotherm of the MgAl-O, 10Ni-O, 20Cr-O and xNi20Cr-O catalysts with different Ni content. (b) Pore size distribution of the MgAl-O, 10Ni-O, 20Cr-O and xNi20Cr-O catalysts with different Ni content.

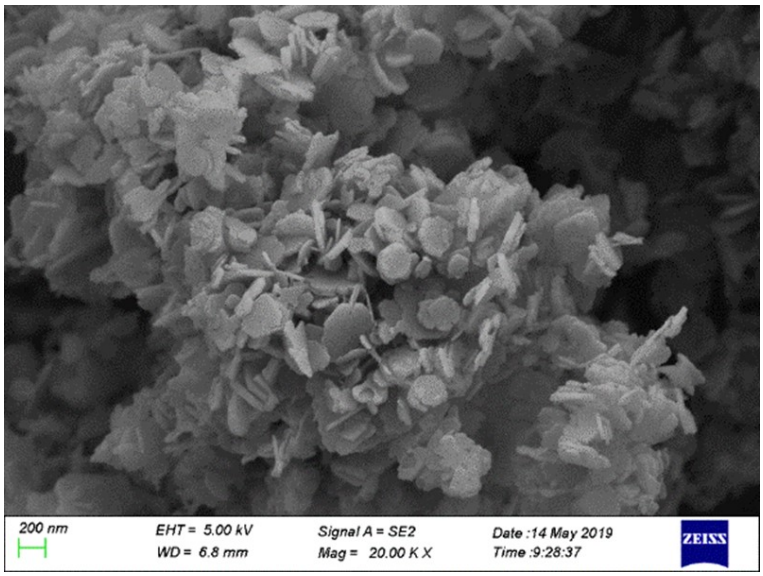

Fig. S3. SEM images of 10Ni20Cr-O catalyst.

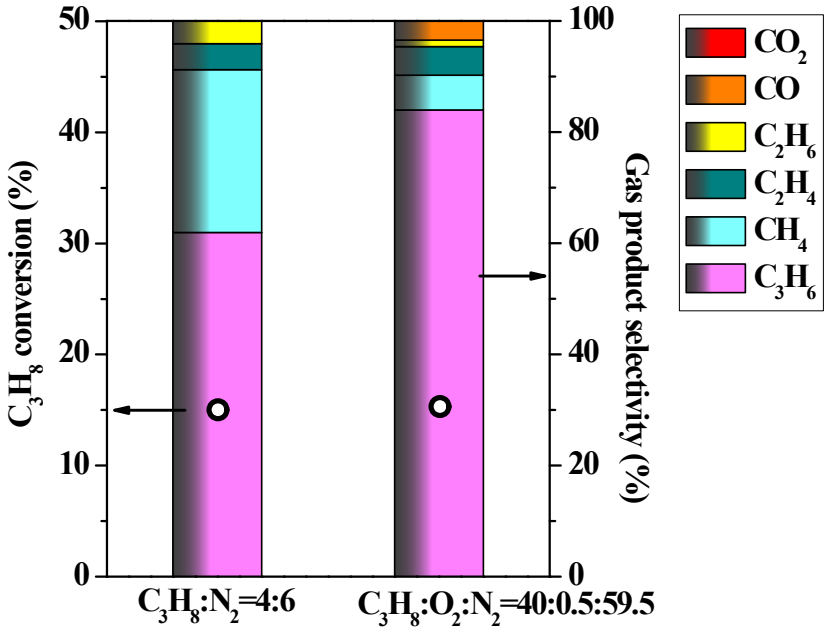

Fig. S4. The C_3H_8 conversion and gas product selectivity of 10Ni20Cr-O catalyst under non-oxidative and oxygen-lean PDH condition after 1h. Reaction condition: 0.1g catalyst, 600 °C, 10 ml/min, C_3H_8/N_2=4:6 or $C_3H_8/O_2/N_2$=40:0.5:59.5.

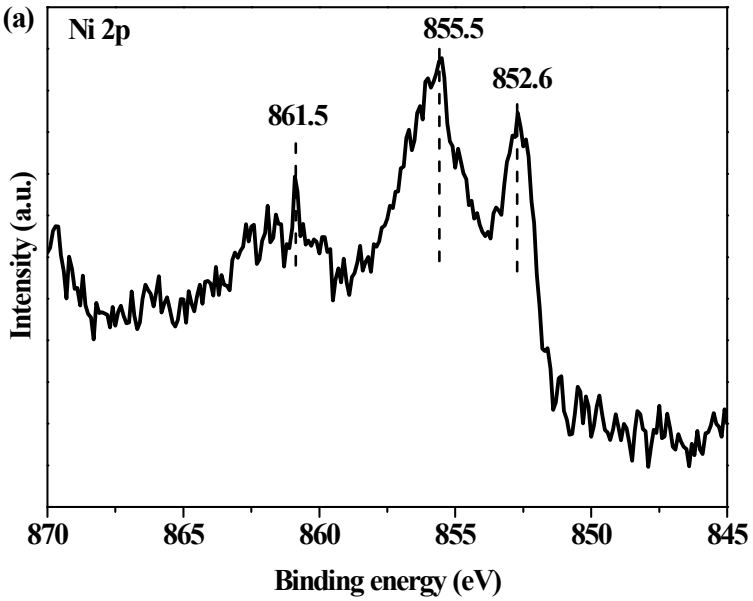

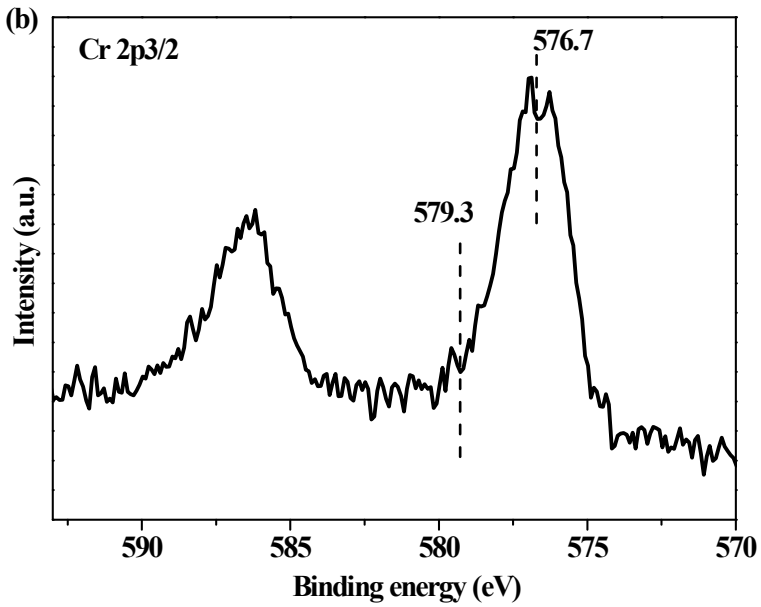

Fig. S5. XPS spectra of Ni 2p (a) and Cr 2p (b) for the spent 10Ni20Cr-O catalyst. Non-oxidation PDH reaction condition: 0.1g catalyst, 600 ^{o}C, 10 ml/min, C_3H_8/N_2=4:6.

The coke selectivity is too low to be detected under the O_2-lean PDH conditions with low C_3H_8 concentration (5 vol %), because the carbon balance of the gas products was almost 100%. The low concentrated C_3H_8 and alkaline MgO support are typically beneficial for the desorption of C_3H_6 and the inhibition of coke formation. Even using an industrially relevant feed with 40 vol % propane, the average coke selectivity of 10Ni20Cr-O catalyst is only 3.4%. The calculation method is as follows: As shown in Fig. S4, the coke mass (m_{coke}) of 0.2 g 10Ni20Cr-O catalyst is 0.0067 g. The amount of C_3H_8 conversion during 5.4 h ($m(C_3H_8)$) can be calculated when the average STY(C_3H_6) is approximate to 0.2 $kg_{C3H6}/(kg_{catal}\cdot h)$ (Fig. S5). The m_{coke}, $n(C_3H_8)$ and the average coke

selectivity can be calculated according to the following formulas:

$m_{coke} = 0.2 \times 3.34\% = 0.0067$ g

$$m(C_3H_8) = \frac{\frac{STY_{C_3H_6}}{S_{C_3H_6}} \times t \times m_{cat}}{} = 0.2/0.9 \times 5.4 \times 0.2 = 0.24 \text{ g}$$

$$\text{Coke selectivity} = \frac{m_{coke}/12}{m(C_3H_8)/44 \times 3} = 3.4\ \%$$

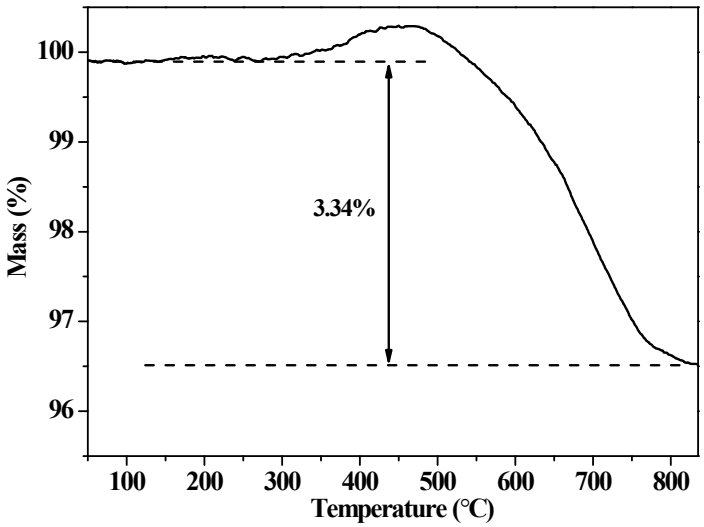

Fig. S6. Thermogravimetry curve of the spent 10Ni20Cr-O catalyst obtained in the O_2 flow (25 ml/min) and heating rate of 10 K/min.

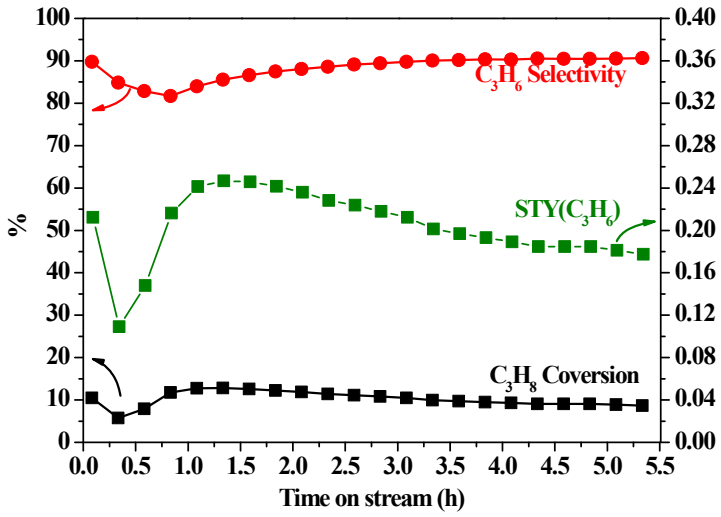

Fig. S7. The C_3H_8 conversion, C_3H_6 selectivity, and STY(C_3H_6) of the reduced 10Ni20Cr-O versus time on stream. Reaction condition: 0.2g

catalyst, 550 °C, 10 ml/min, $C_3H_8/O_2/N_2$=40:0.5:59.

Fig. 8 shows the coke Raman peak intensity of 10Cr20Ni-O catalyst under high and low concentration C_3H_8 reaction condition, the former is almost five times more than the latter. These suggest that the amount of coke formation at low propane concentration condition is significantly lower than that at high propane concentration condition. Coke property of the two spent catalysts was also evaluated by the intensity ratio of the D_1 band to the G band (I_{D1}/I_G). Their I_{D1}/I_G value are both around 1, indicating the same graphite crystallinity.

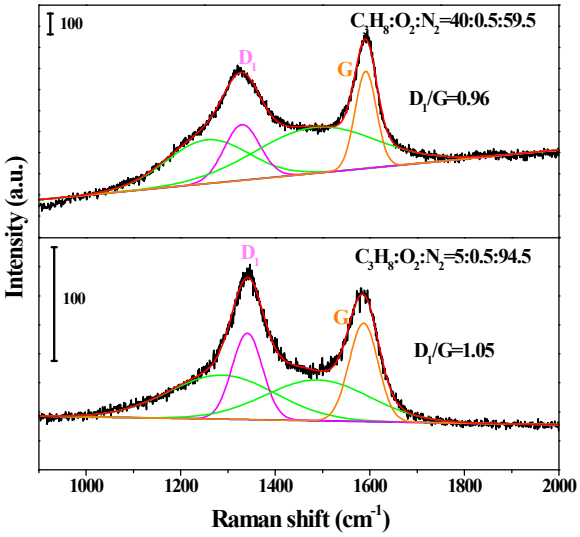

Fig. S8. Raman spectra of spent 10Cr20Ni-O catalyst under different C_3H_8 concentration (up: $C_3H_8/O_2/N_2$=40:0.5:59.5, down $C_3H_8/O_2/N_2$=5:0.5:94.5) after 5.4 h reaction at 550 °C (total flow 10 ml/min).

Table S1. BET specific surface area, pore size and pore volume of the MgAl-O, 10Ni-O, 20Cr-O and xNi20Cr-O catalysts.

Samples	$S_{BET}(m^2/g)^a$	$V_p\ (cm^3/g)^b$	$D_p\ (nm)^c$
MgAl-O	185.1	0.68	16.5
10Ni-O	195.7	0.54	13.1
20Cr-O	189.0	0.50	8.0
5Ni20Cr-O	254.0	0.41	5.0
10Ni20Cr-O	244.7	0.42	6.0
20Ni20Cr-O	267.0	0.36	4.1

[a]: S_{BET} is the specific surface area calculated by BET method.

[b]: V_P is the total pore volume.

[c]: D_p is the average pore diameter determined from the desorption branches of the nitrogen sorption isotherms according to the BJH method (Fig. S1b).

Table S2. The catalytic performance of the 10Ni-O, 20Cr-O and xNi20Cr-O catalysts for oxygen-lean propane dehydrogenation.

Catalyst	Time on stream (min)	Conversion (%)	Selective (%)						C_3H_6 yield (%)	CO_x yield (%)
			CO	CH_4	CO_2	C_2H_4	C_2H_6	C_3H_6		
Empty tube	-	1.1	0.6	14.3	1.8	31.6	0.0	51.7	0.6	0.03
10Ni-O	5	30.5	22.6	0.9	33.7	20.2	0.0	22.6	6.9	17.2
10Ni-O	305	1.8	2.5	9.5	10.6	26.8	0.0	50.6	0.9	0.2
20Cr-O	5	9.6	2.6	4.4	6.9	3.9	0.3	82.0	7.9	0.9
20Cr-O	305	5.0	1.2	4.3	2.3	6.4	0.3	85.6	4.3	0.2
5Ni20Cr-O	5	16.8	5.7	4.5	26.1	3.0	0.0	60.7	10.2	5.3
5Ni20Cr-O	305	11.9	2.7	2.3	1.5	2.0	0.0	91.5	10.9	0.5
10Ni20Cr-O	80	19.1	57.7	27.6	1.1	0.4	2.0	11.2	2.1	11.2
10Ni20Cr-O	305	33.7	5.4	3.3	0.0	1.2	0.6	89.5	30.2	1.8
20Ni20Cr-O	65	79.4	27.3	72.2	0.4	0.0	0.0	0.0	0.0	22.0
20Ni20Cr-O	305	6.1	63.4	35.8	0.0	0.8	0.0	0.0	0.0	3.8

Table S3. Catalytic performance of various catalysts from literature in the propane dehydrogenation.

Catalyst	m/g	T/°C	Conversion (C_3H_8)	Selectivity (C_3H_6)	F_{total}/ mL·min^{-1}	Feeding gas composition	WHSV / h^{-1}	STY(C_3H_6) /kg·h^{-1}·kg^{-1}	k_d	Ref.
ZrO_2	0.07	550	28.4	87.0	10	40 vol% C_3H_8 in N_2	6.7	1.58	0.7	1
ZrO_2	0.08	600	28.3	85.5	20	40 vol% C_3H_8 in N_2	11.7	2.71	3.7	1
2.5%Si@PtGa /Al_2O_3	0.1	450	21.0	92.0	40	$C_3H_8/H_2/N_2$=2.5:2.5:95	1.2	0.21	0.007	2
$PtZn_4$@S-1-H	0.3	550	47.4	93.2	40	25 vol% C_3H_8 in N_2	3.6	1.59	0.072	3
VO_x/Al_2O_3	0.25	600	32.0	94	25	28 vol% C_3H_8, 28% H_2 in N_2	3.0	0.86	0.5-1.6	4, 5
$7Cr/ZrO_2$	0.2	550	68	60	20	$C_3H_8/CO_2/N_2$=1/2/37	0.3	0.12	0.28	6
K-CrO_x/Al_2O_3	-	550	29	90	10	40 vol% C_3H_8 in N_2	-	2.64	0.455	7
$Cr_{10}Zr_{90}/SiO_2$	-	600	-	-	-	40 vol% C_3H_8 in N_2	11.52	2.4	1.2	8
Cr-Al-800	0.1	600	33.2	90.4	8	Pure C_3H_8	9.4	2.6	0.28	9
Sn-HMS	1.5	600	40.0	90.0	5	Pure C_3H_8	0.39	0.14	4.2×10^{-4}	10
VO_x(5)/MCM -41	-	570	45	88	-	$C_3H_8/O_2/N_2$=15/0.5/84.5	0.64	0.23	0.015	11
Zn-S-1_3	-	550	31	96	-	40 vol% C_3H_8 in N_2	7.9	2.1	1.5	12

Zn-S-1_3	-	600	38	96	-	40 vol% C_3H_8 in N_2	15.8	5.8	4.5	12
10Ni20Cr-O	0.2	550	34	89	10	$C_3H_8/O_2/N_2$=5:0.5:94.5	0.06	0.02	0.02	This work
10Ni20Cr-O	0.2	550	12.4	88.3	10	$C_3H_8/O_2/N_2$= 40:0.5:59.5	2.4	0.25	0.11	This work
10Ni20Cr-O	0.1	600	15	84	10	$C_3H_8/O_2/N_2$= 40:0.5:59.5	4.8	0.6	0.22	This work

References

(1) Zhang, Y.; Zhao, Y.; Otroshchenko, T.; Lund, H.; Pohl, M.-M.; Rodemerck, U.; Linke, D.; Jiao, H.; Jiang, G.; Kondratenko, E. V. Control of Coordinatively Unsaturated Zr sites in ZrO_2 for Efficient C–H bond activation. *Nat. Commun.* **2018**, *9*, 3794-3804.

(2) Wang, P.; Yao, J.; Jiang, Q.; Gao, X.; Lin, D.; Yang, H.; Wu, L.; Tang, Y.; Tan, L. Stabilizing the isolated Pt sites on PtGa/Al_2O_3 catalyst via silica coating layers for propane dehydrogenation at low temperature. *Applied Catalysis B: Environmental* **2022**, *300*, 120731.

(3) Sun, Q.; Wang, N.; Fan, Q.; Zeng, L.; Mayoral, A.; Miao, S.; Yang, R.; Jiang, Z.; Zhou, W.; Zhang, J.; Zhang, T.; Xu, J.; Zhang, P.; Cheng, J.; Yang, D.-C.; Jia, R.; Li, L.; Zhang, Q.; Wang, Y.; Terasaki, O.; Yu, J., Subnanometer Bimetallic Pt-Zn Clusters in Zeolites for Propane Dehydrogenation. *Angew. Chem. Int. Ed.* **2020**, 59, 19450-19459.

(4) Liu, G.; Zhao, Z.-J.; Wu, T.; Zeng, L.; Gong, J. Nature of the Active Sites of VO_x/Al_2O_3 Catalysts for Propane Dehydrogenation. *ACS Catal.* **2016**, *6*, 5207-5214.

(5) Zhao, Z.-J.; Wu, T.; Xiong, C.; Sun, G.; Mu, R.; Zeng, L.; Gong, J. Hydroxyl-Mediated Non-oxidative Propane Dehydrogenation over VOx/γ-Al_2O_3 Catalysts with Improved Stability. *Angew. Chem. Int. Ed.* **2018**, *57* (23), 6791-6795

(6) Xie, Z.; Ren, Y.; Li, J.; Zhao, Z.; Fan, X.; Liu, B.; Song, W.; Kong, L.; Xiao, X.; Liu, J.; et al. Facile in situ synthesis of highly dispersed chromium oxide incorporated into mesoporous ZrO_2 for the dehydrogenation of propane with CO_2. *J. Catal.* **2019**, *372*, 206-216.
(7) Otroshchenko, T. P.; Rodemerck U.; Linke D.; Kondratenko, E. V. Synergy effect between Zr and Cr active sites in binary CrZrOx or supported CrOx/LaZrOx: Consequences for catalyst activity, selectivity and durability in non-oxidative propane dehydrogenation. *J. Catal.* **2017**, *356*, 197–205.
(8) Han, S.; Zhao, Y.; Otroshchenko, T.; Zhang, Y.; Zhao, D.; Lund, H.; Vuong, T. H.; Rabeah, J.; Bentrup, U.; Kondratenko, V. A.; et al. Unraveling the Origins of the Synergy Effect between ZrO_2 and CrOx in Supported CrZrOx for Propene Formation in Nonoxidative Propane Dehydrogenation. *ACS Catal.* **2020**, *10* (2), 1575-1590.
(9) Gao, X.-Q.; Lu, W.-D.; Hu, S.-Z.; Li, W.-C.; Lu, A.-H. Rod-shaped porous alumina-supported Cr_2O_3 catalyst with low acidity for propane dehydrogenation. *Chinese J. Catal.* **2019**, *40* (2), 184-191.
(10) Wang, G.; Zhang, H.; Zhu, Q.; Zhu, X.; Li, X.; Wang, H.; Li, C.; Shan, H., Sn-containing Hexagonal Mesoporous Silica (HMS) for Catalytic Dehydrogenation of Propane: An Efficient Strategy to Enhance Stability. *J. Catal.* **2017**, *351*, 90-94.
(11) Ovsitser, O.; Schomaecker, R.; Kondratenko, E. V.; Wolfram, T.; Trunschke, A. Highly selective and stable propane dehydrogenation to propene over dispersed VOx-species under oxygen-free and oxygen-lean conditions. *Catal. Today* **2012**, *192* (1), 16-19.
(12) Zhao, D.; Tian, X.; Doronkin, D. E.; Han, S.; Kondratenko, V. A.; Grunwaldt, J.-D.; Perechodjuk, A.; Vuong, T. H.; Rabeah, J.; Eckelt, R.; et al. In situ formation of ZnOx species for efficient propane dehydrogenation. *Nature* **2021**, 599 (7884), 234-238.